The Astrophysical Journal, 718:575–582, 2010 July 20 doi:10.1088/0004-637X/718/1/575

THE HAT-P-13 EXOPLANETARY SYSTEM: EVIDENCE FOR SPIN–ORBIT ALIGNMENT AND A THIRD COMPANION

Joshua N. Winn[1,2], John Asher Johnson[3], Andrew W. Howard[4,5,8], Geoffrey W. Marcy[4], Gáspár Á. Bakos[6,9], Joel Hartman[6], Guillermo Torres[6], Simon Albrecht[1], and Norio Narita[2,7]

[1] Department of Physics, and Kavli Institute for Astrophysics and Space Research, Massachusetts Institute of Technology, Cambridge, MA 02139, USA
[2] Kavli Institute for Theoretical Physics, UCSB, Santa Barbara, CA 93106, USA
[3] Department of Astrophysics, California Institute of Technology, MC 249-17, Pasadena, CA 91125, USA
[4] Department of Astronomy, University of California, Mail Code 3411, Berkeley, CA 94720, USA
[5] Space Sciences Laboratory, University of California, Berkeley, CA 94720, USA
[6] Harvard-Smithsonian Center for Astrophysics, 60 Garden Street, Cambridge, MA 02138, USA
[7] National Astronomical Observatory of Japan, 2-21-1 Osawa, Mitaka, Tokyo 181-8588, Japan
Received 2010 March 23; accepted 2010 May 28; published 2010 July 1

ABSTRACT

We present new radial velocity (RV) measurements of HAT-P-13, a star with two previously known companions: a transiting giant planet "b" with an orbital period of 3 days and a more massive object "c" on a 1.2 yr, highly eccentric orbit. For this system, dynamical considerations would lead to constraints on planet b's interior structure, if it could be shown that the orbits are coplanar and apsidally locked. By modeling the Rossiter–McLaughlin effect, we show that planet b's orbital angular momentum vector and the stellar spin vector are well aligned on the sky ($\lambda = 1.9 \pm 8.6$ deg). The refined orbital solution favors a slightly eccentric orbit for planet b ($e = 0.0133 \pm 0.0041$), although it is not clear whether it is apsidally locked with c's orbit ($\Delta\omega = 36^{+27}_{-36}$ deg). We find a long-term trend in the star's RV and interpret it as evidence for an additional body "d," which may be another planet or a low-mass star. Predictions are given for the next few inferior conjunctions of c, when transits may happen.

Key words: planets and satellites: dynamical evolution and stability – planets and satellites: formation – planets and satellites: individual (HAT-P-13b, c, d) – planets and satellites: interiors – stars: rotation

Online-only material: color figure

1. INTRODUCTION

Precise radial velocity (RV) measurements have revealed more than 30 multiple-planet systems (Wright 2010). However, in only a few cases have transits been detected for any of the planets in those systems. Those cases are potentially valuable because the transit observables—the times of conjunction, orbital inclination, and projected spin–orbit angle, among others—provide a much more complete description of a planetary system, which may in turn give clues about its formation and evolution. The Corot-7 system has two orbiting super-Earths, one of which transits (Léger et al. 2009; Queloz et al. 2009). The HAT-P-7 system has a transiting hot Jupiter in a polar or retrograde orbit, as well as a longer-period companion that could be a planet or a star (Pál et al. 2008; Winn et al. 2009; Narita et al. 2010). The HAT-P-13 system, the subject of this paper, features a G4 dwarf star with two previously known orbiting companions (Bakos et al. 2009). The inner companion (HAT-P-13b, or simply "b" hereafter) is a transiting hot Jupiter in a 2.9 day orbit. The outer companion ("c") has an eccentric 1.2 yr orbit and a minimum mass ($M_c \sin i_c$) of about 15 Jupiter masses, although its true mass (M_c) and orbital inclination (i_c) are unknown. In particular, transits of companion c have neither been observed nor ruled out.

Batygin et al. (2009) and Mardling (2010) showed that it may be possible to use the observed state of the system to determine planet b's Love number k_2, a parameter that depends on the planet's interior density distribution. This would be of great interest, as few other methods exist for investigating the interior structure of exoplanets. The method is based on the theoretical expectation that tidal evolution has aligned the apsides of the orbits of b and c. This method has not yet yielded meaningful constraints on k_2, partly because of the large uncertainty in the eccentricity of b's orbit. Another relevant parameter is the mutual inclination between the orbits, which is not known at all.

RV observations are usually powerless to determine mutual inclinations, unless the planets are in a mean-motion resonance (see, e.g., Correia et al. 2010). However, for a transiting planet it is possible to assess the alignment between the orbit and the stellar equator through the Rossiter–McLaughlin (RM) effect. A system with mutually inclined planetary orbits might also be expected to have large angles between the orbits and the stellar equator. In particular, Mardling (2010) presented a formation scenario for HAT-P-13 involving gravitational scattering by a putative third companion, which could have caused large mutual inclinations and a large stellar obliquity.

In this paper, we present new RV measurements of HAT-P-13 bearing on all these issues. The new data are presented in Section 2. Our analysis is presented in Section 3, and includes evidence for a third companion "d" (Section 3.1), refined estimates of the eccentricity and apsidal orientation of b's orbit (Section 3.2), modeling of the RM effect (Section 3.3), and updated predictions for the next inferior conjunction (possible transit window) of companion c (Section 3.4). In Section 4, we discuss the implications for further dynamical investigations of HAT-P-13.

2. OBSERVATIONS

We observed HAT-P-13 with the High Resolution Spectrograph (HIRES; Vogt et al. 1994) on the Keck I 10 m telescope,

[8] Townes Postdoctoral Fellow.
[9] NSF Fellow.

Table 1
Relative Radial Velocity Measurements of HAT-P-13

BJD	RV (m s^{-1})	Error (m s^{-1})
2454548.80650	87.29	2.00
2454548.90850	70.55	1.44
2454602.73396	−77.76	1.49
2454602.84691	−77.84	1.72
2454603.73415	82.29	1.41
2454603.84324	102.65	2.05
2454633.77241	112.70	2.00
2454634.75907	−57.09	1.97
2454635.75475	86.55	2.12
2454636.74969	107.21	1.80
2454727.13850	117.62	1.90
2454728.13189	−58.37	1.66
2454778.07301	−57.70	1.40
2454779.08373	120.17	1.71
2454780.09368	−13.75	1.88
2454791.11129	92.67	1.64
2454809.99575	−114.15	2.39
2454839.06085	−225.51	1.54
2454865.02660	−448.40	1.49
2454867.90311	−488.00	2.88
2454928.83635	−289.10	1.44
2454955.86964	−186.54	1.63
2454956.86327	−5.48	1.90
2454963.85163	−119.86	1.62
2454983.74976	41.30	1.50
2454984.76460	−134.63	1.51
2454985.73856	19.77	1.50
2454986.76358	25.83	1.75
2454988.74066	50.77	1.68
2455109.11745	143.40	2.24
2455110.10818	−30.20	2.91
2455134.11719	48.56	1.55
2455135.13125	168.31	1.97
2455164.01155	181.07	2.06
2455172.12118	72.55	1.78
2455173.02454	172.95	1.73
2455188.04447	102.62	1.53
2455189.08587	−25.28	1.29
2455189.98539	140.26	1.30
2455191.11450	67.47	1.49
2455192.02847	−33.41	1.50
2455193.85943	105.31	1.49
2455193.86475	104.10	1.48
2455193.86961	97.82	1.49
2455193.94390	87.20	1.50
2455193.94850	84.10	1.68
2455193.95323	81.03	1.59
2455193.95775	81.95	1.49
2455193.96234	85.47	1.61
2455193.96702	73.88	1.69
2455193.97167	84.75	1.63
2455193.97628	79.58	1.59
2455193.98097	80.27	1.64
2455193.98536	85.58	1.44
2455193.98980	80.71	1.51
2455193.99433	79.41	1.42
2455193.99888	81.14	1.59
2455194.00354	73.98	1.60
2455194.00825	79.68	1.49
2455194.01271	72.95	1.60
2455194.01716	73.63	1.54
2455194.02147	71.22	1.49
2455194.02618	72.92	1.45
2455194.03098	64.82	1.55
2455194.03561	64.92	1.54
2455194.04057	66.44	1.55
2455194.04546	67.07	1.62
2455194.05048	64.00	1.51
2455194.05515	54.30	1.56
2455194.05976	56.32	1.60
2455194.06437	61.63	1.46
2455194.06915	51.66	1.52
2455194.07416	49.80	1.63
2455194.07901	50.00	1.50
2455194.08376	53.07	1.52
2455194.08858	46.90	1.47
2455194.09350	51.24	1.63
2455194.09842	51.69	1.50
2455194.10345	51.65	1.65
2455194.10848	54.47	1.68
2455194.11341	48.28	1.54
2455194.11813	43.50	1.59
2455194.12270	49.47	1.51
2455194.12732	47.17	1.63
2455194.13216	47.26	1.57
2455194.13716	41.20	1.51
2455194.17667	33.41	1.44
2455196.94719	59.88	1.29
2455197.94842	−36.39	2.02
2455229.08581	20.75	1.66
2455229.87780	−60.13	1.73
2455232.01621	22.91	1.52
2455251.92524	96.71	2.09
2455255.82341	−93.36	1.40
2455256.97046	54.58	1.47
2455260.85979	39.52	1.54
2455284.82534	−171.99	1.73
2455285.89491	−97.21	1.75
2455289.81794	−32.19	1.31
2455311.74995	−418.30	1.56
2455312.83027	−254.42	1.53
2455313.74879	−405.93	1.39
2455314.80031	−436.91	1.87
2455320.86712	−514.39	1.58
2455321.81620	−436.55	1.73

Notes. The RV was measured relative to an arbitrary template spectrum; only the differences are significant. The uncertainty given in Column 3 is the internal error only and does not account for "stellar jitter."

using the same instrument settings and observing protocols that were used by Bakos et al. (2009) and are used by the California Planet Search (Howard et al. 2009). In particular, we used the iodine gas absorption cell to calibrate the instrumental point-spread function and the wavelength scale. The total number of new spectra is 75, which are added to the 30 spectra presented by Bakos et al. (2009). Of the new spectra, 40 were obtained on the night of 2009 December 27–28, spanning a transit of HAT-P-13b, and were gathered to measure the RM effect. The other 35 were obtained on arbitrary nights. They extend the timespan of the data set by approximately 1 yr, and thereby help to refine the orbital parameters.

The RV of each spectrum was measured with respect to an iodine-free template spectrum, using the algorithm of Butler et al. (1996) with subsequent improvements. All of the spectra obtained by Bakos et al. (2009) were re-reduced, for consistency. Measurement errors were estimated from the scatter in the fits to individual spectral segments spanning 2 Å. The RVs are given in Table 1, and plotted as a function of time in Figures 1 and 2.

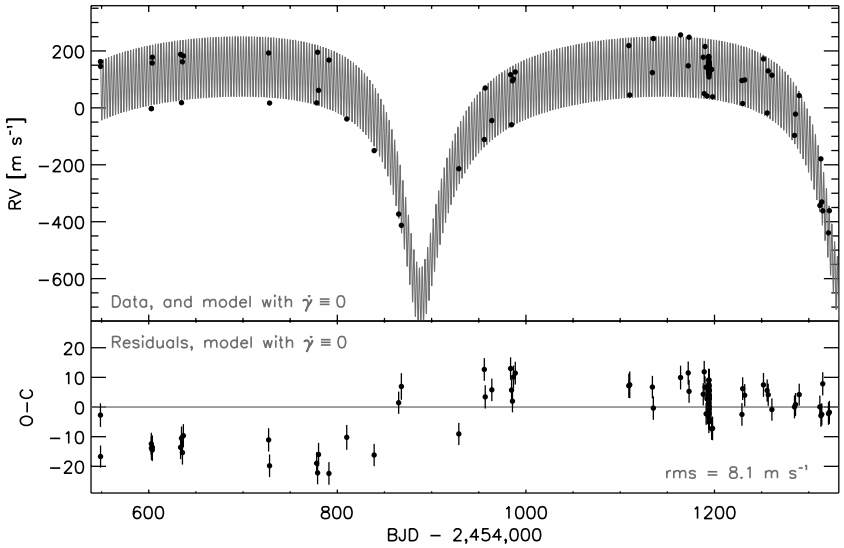

Figure 1. RV variation of HAT-P-13. Top: measured RVs, and the best-fitting model. The model consisted of two Keplerian orbits and did not allow for any additional acceleration ($\dot{\gamma} \equiv 0$). Bottom: residuals. The poorness of the fit, and the pattern of residuals, are evidence for a third companion.

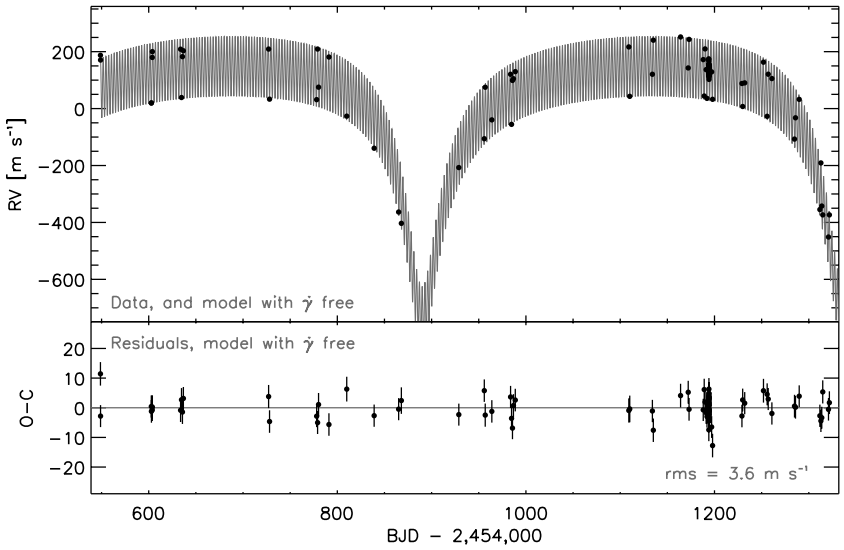

Figure 2. RV variation of HAT-P-13. Top: measured RVs, and the best-fitting model, this time allowing for a constant radial acceleration ($\dot{\gamma}$) in addition to two Keplerian orbits. The best-fitting value of $\dot{\gamma}$ was 17.5 m s^{-1} yr^{-1}. Bottom: residuals.

The model curves appearing in those figures are explained in Section 3.

3. ANALYSIS

Our model for the RV data took the form

$$V_{\rm calc}(t) = V_{\rm b}(t) + V_{\rm c}(t) + V_{\rm RM}(t) + \gamma + \dot{\gamma}(t - t_0), \quad (1)$$

where $V_{\rm calc}$ is the calculated RV, $V_{\rm b}$ and $V_{\rm c}$ are the RVs of non-interacting Keplerian orbits, $V_{\rm RM}$ is the transit-specific "anomalous velocity" due to the RM effect (Section 3.3), and $\{\gamma, \dot{\gamma}, t_0\}$ are constants. The first constant, γ, specifies the velocity offset between the system barycenter and the arbitrary template spectrum that was used to calculate RVs. The second constant, $\dot{\gamma}$, allows for a constant radial acceleration, and was included because models with $\dot{\gamma} = 0$ did not fit the data (Section 3.1). We interpret $\dot{\gamma}$ as the acceleration produced by a newly discovered long-period companion "d." The third constant, t_0, is an arbitrary reference time that was taken to be the time of the first RV datum (BJD 2,454,548.80650).

Our RM model was based on that of Winn et al. (2005), in which simulated spectra are used to calibrate the relation between the phase of the transit and the measured RV. For this case, we used the relation

$$\Delta V(t) = -(v \sin i_\star)\delta(t)\left[0.9833 - 0.0356\left(\frac{v_p(t)}{v \sin i_\star}\right)^2\right], \quad (2)$$

where $v \sin i_\star$ is the sky-projected stellar rotation speed, δ is the fractional loss of light, and v_p is the RV of the portion of the stellar photosphere that is hidden by the planet. To calculate v_p, we assumed that the stellar photosphere rotates uniformly with an angle λ between the sky projections of the spin vector and the orbital angular momentum vector (see, e.g., Ohta et al. 2005; Gaudi & Winn 2007).

Since δ depends on the planet-to-star radius ratio $R_p/R_\star$, orbital inclination i, and impact parameter $b_{\rm tra}$, all of which are more tightly bounded by observations of photometric transits than by the RM effect, we simultaneously fitted a composite i'-

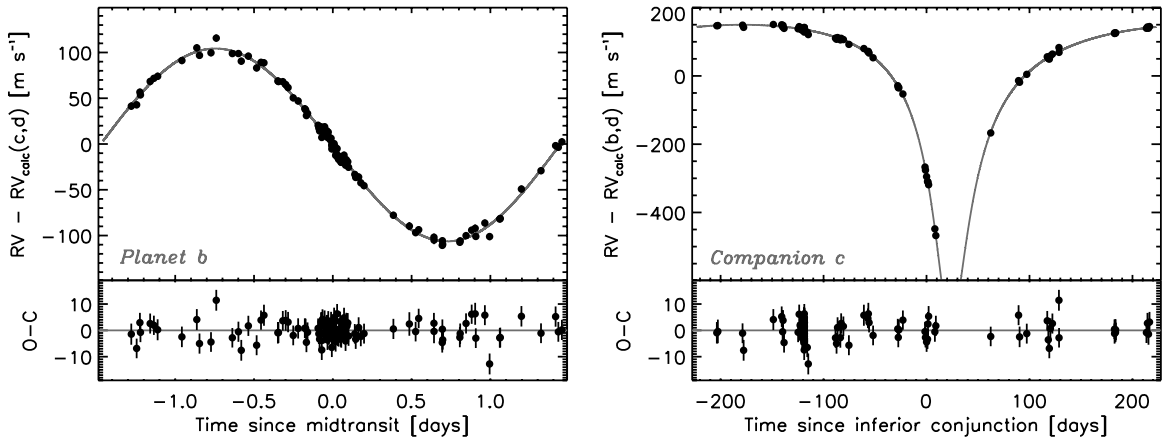

Figure 3. RV variation as a function of orbital phase. Left: RV variation as a function of the orbital phase of planet b after subtracting the calculated variation due to c and d. Right: RV variation as a function of the orbital phase of c, after subtracting the calculated variation due to b and d.

band transit light curve based on the photometric data of Bakos et al. (2009). For the photometric model we assumed a quadratic limb-darkening law and used the analytic formula of Mandel & Agol (2002), as implemented by Pál (2008). Because the photometric data are not precise enough to constrain both of the limb-darkening coefficients u_1 and u_2, we fixed $u_2 \equiv 0.3251$, the value obtained by interpolating the Claret (2004) tables, and allowed u_1 to vary freely.[10] For the RM model, we used a linear law with a fixed coefficient of 0.72, as appropriate for the V band, the approximate spectral range from which the RV signal is drawn.

All together there were 18 adjustable parameters, of which 12 were controlled almost exclusively by the RV data and 6 by the photometric data. The data set had 105 RVs and 107 flux data points. Thus, the total number of degrees of freedom was 194, of which 93 pertained to RVs and 101 to photometry.

We determined the best-fitting parameter values and their 68.3% confidence limits with a Monte Carlo Markov Chain (MCMC) algorithm that we have described elsewhere (see, e.g., Winn et al. 2007). Uniform priors were adopted for all parameters except for b's time of transit and orbital period, for which we adopted Gaussian priors based on the ephemeris of Bakos et al. (2009). We doubled the quoted errors in the ephemeris, out of concern that systematic errors or transit-timing variations have affected the results. The likelihood was taken to be $\exp(-\chi^2/2)$ with

$$\chi^2 = \sum_{i=1}^{105}\left[\frac{v_i(\mathrm{obs}) - v_i(\mathrm{calc})}{\sigma_i}\right]^2 + \sum_{j=1}^{107}\left[\frac{f_j(\mathrm{obs}) - f_j(\mathrm{calc})}{\sigma_j}\right]^2 = \chi^2_v + \chi^2_f, \qquad (3)$$

where v_i(obs) and σ_i are the RV data and associated uncertainties, v_i(calc) are the calculated RVs, f_j(obs) and σ_j are the flux data and associated uncertainties, and f_j(calc) are the calculated fluxes.

Each flux uncertainty σ_i was taken to be the scatter in the ≈16 data points contributing to each 4 minute time bin. Each RV uncertainty σ_j was taken to be the quadrature sum of the internally estimated measurement error and a "jitter" term of 3.4 m s^{-1}. The jitter term was set by the requirement $\chi^2_v = 93$, the relevant number of degrees of freedom, and is consistent with the empirical jitter estimates of Wright (2005) for stars similar to HAT-P-13. In the best-fitting model, $\chi^2_f = 109.5$ and $\chi^2_v = 93.0$, the rms photometric residual was 470 ppm and the rms RV residual was 3.6 m s^{-1}.

Table 2 gives the results for the parameter values. Figure 3 shows the RVs as a function of the orbital phases of b and

[10] The result, $u_1 = 0.269 \pm 0.076$, was consistent with the tabulated value of 0.3068.

Table 2
Model Parameters for HAT-P-13

Parameter	Value
Star	
Mass, $M_\star$ ($M_\odot$)	$1.22^{+0.05}_{-0.10}$
Radius, $R_\star$ ($R_\odot$)	1.559 ± 0.080
Projected stellar rotation rate, $v \sin i_\star$ (km s^{-1})	1.66 ± 0.37
Planet b	
Mass, M_b ($M_{\rm Jup}$)	0.851 ± 0.038
Radius, R_b ($R_{\rm Jup}$)	1.272 ± 0.065
Orbital period, P_b (days)	2.916250 ± 0.000015
Planet-to-star radius ratio, $R_p/R_\star$	0.08389 ± 0.00081
Star-to-orbit radius ratio, $R_\star/a$	0.1697 ± 0.0072
Orbital inclination, i (deg)	83.40 ± 0.68
Impact parameter, $b_{\rm tra}$	0.679 ± 0.043
Time of midtransit, $T_{{\rm tra},b}$ (BJD)	2454779.92976 ± 0.00075
Orbital eccentricity, e_b	0.0133 ± 0.0041
Argument of pericenter, ω_b (deg)	210^{+27}_{-36}
$e_b \cos\omega_b$	−0.0099 ± 0.0036
$e_b \sin\omega_b$	−0.0060 ± 0.0069
Velocity semiamplitude, K_b (m s^{-1})	106.04 ± 0.73
Projected spin–orbit angle, λ (deg)	1.9 ± 8.6
Companion c	
Minimum mass, $M_c \sin i_c$ ($M_{\rm Jup}$)	14.28 ± 0.28
Orbital period, P_c (days)	446.27 ± 0.22
Time of inferior conjunction, $T_{{\rm con},c}$ (BJD)	2455312.80 ± 0.74
Orbital eccentricity, e_c	0.6616 ± 0.0054
Argument of pericenter, ω_c (deg)	175.29 ± 0.35
$e_c \cos\omega_c$	−0.6594 ± 0.0056
$e_c \sin\omega_c$	0.0543 ± 0.0038
Velocity semiamplitude, K_c (m s^{-1})	440 ± 11
Other system parameters	
Angle between apsides, $\omega_b - \omega_c$ (deg)	36^{+27}_{-36}
Velocity offset, γ (m s^{-1})	−100.3 ± 2.0
$\dot\gamma$ (m s^{-1} yr^{-1})	17.51 ± 0.90

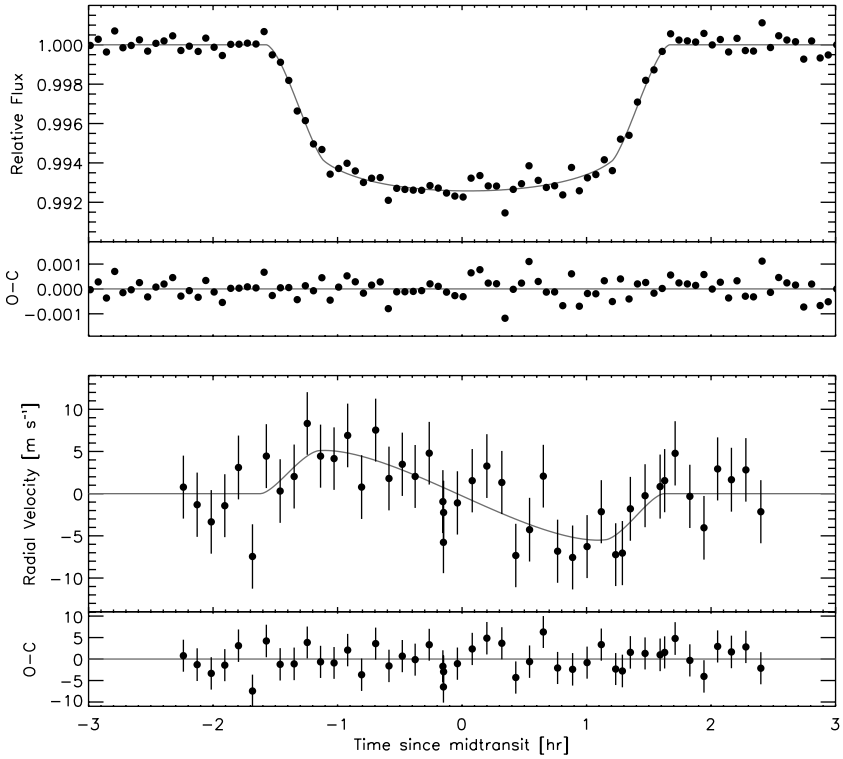

Figure 4. Transit photometry and RV variation. Top: composite transit light curve based on the i'-band photometric data of Bakos et al. (2009). Also plotted are the best-fitting model and the residuals. Bottom: apparent RV variation observed during the transit phase, after subtracting the calculated contributions due to orbital motion. The observed variation is interpreted as the anomalous velocity due to the RM effect.

c, expressed in days. In the left panel, the RVs are plotted as a function of the orbital phase of b, after subtracting the calculated contributions to the RV from companions c and d. (The contribution due to d is a linear function of time.) Likewise, the right panel of Figure 3 shows the RVs as a function of the orbital phase of c, after subtracting the calculated contributions from b and d. Figure 4 shows the data over a restricted time range centered on b's transit. The top panel shows the light curve. The bottom panel shows the data after subtracting the calculated orbital RV, thereby isolating the RM effect.

3.1. Evidence for a Third Companion

The extra acceleration, $\dot{\gamma}$, was included in the RV model because a model consisting of only two Keplerian orbits gave an unacceptable fit to the data. With $\dot{\gamma} = 0$, the RV-specific portions of the data and model had $\chi^2_v = 458.6$ and 94 degrees of freedom ($\chi^2_v / N_{\mathrm{dof},v} = 4.9$). The pattern of residuals is displayed in Figure 1. There are large and time-correlated residuals that are not easily attributed to stellar jitter or underestimated measurement errors.

In contrast, when $\dot{\gamma}$ was allowed to vary freely, the best-fitting model had $\dot{\gamma} = 17.5$ m s^{-1} yr^{-1}, and $\chi^2_v = 93$ with 93 degrees of freedom. The exact match between χ^2_v and $N_{\mathrm{dof},v}$ is not significant in itself, as it follows from our choice of 3.4 m s^{-1} for the jitter term. However, it is significant that an acceptable fit was found for a choice of jitter term that is in line with observations of similar stars. Even more significant is that the correlated pattern of residuals vanished. As shown in Figure 2, the residuals scattered randomly around zero.

The failure of the two-Keplerian model, and the success of a model with an additional radial acceleration, is evidence for a third companion to HAT-P-13 ("d") with a long orbital period. With the limited information available, though, the properties of d are largely unknown. Assuming its orbit to be nearly circular, and its mass to be much smaller than that of the star, we may set $\dot{\gamma} \sim G M_d \sin i_d / a_d^2$ to give an order-of-magnitude constraint

$$\left(\frac{M_d \sin i_d}{M_{\mathrm{Jup}}}\right)\left(\frac{a_d}{10\mathrm{AU}}\right)^{-2} \sim 9.8, \qquad (4)$$

where a_d is the orbital distance. By this standard, the newly discovered object could be a 2.5 M_{Jup} planet at 5 AU, or a 10 M_{Jup} planet at 10 AU, or a 90 M_{Jup} (0.09 $M_\odot$) star at 30 AU, etc. The properties of d could be substantially different depending on its eccentricity, argument of pericenter, and time of conjunction. Orbits closer than ∼5 AU would be subject to additional constraints by the requirement of dynamical stability.

More information about d could be gleaned from any significant *curvature* in the RV signal, beyond the effects of the two Keplerian orbits and a linear trend. We experimented with models that include a "jerk" parameter, $\ddot{\gamma}$, finding this parameter to be highly covariant with the mass, orbital period, and eccentricity of c. More elaborate models and detailed constraints on companion d will only be justified after another few years of observing, when the properties of companion c will have been well established. The uncertainties given in Table 2 must therefore be understood as subject to the assumption that d is producing no significant RV curvature.

3.2. Orbital Eccentricities

Figure 5 shows the results for the orbital eccentricities. Planet c's orbit is strongly eccentric, with $e_c = 0.6616 \pm 0.0054$. Planet b's orbit is nearly circular, with $e_b = 0.0133 \pm 0.0041$. To assess the significance of the detection of eccentricity, it is simpler to examine the components of the eccentricity vector

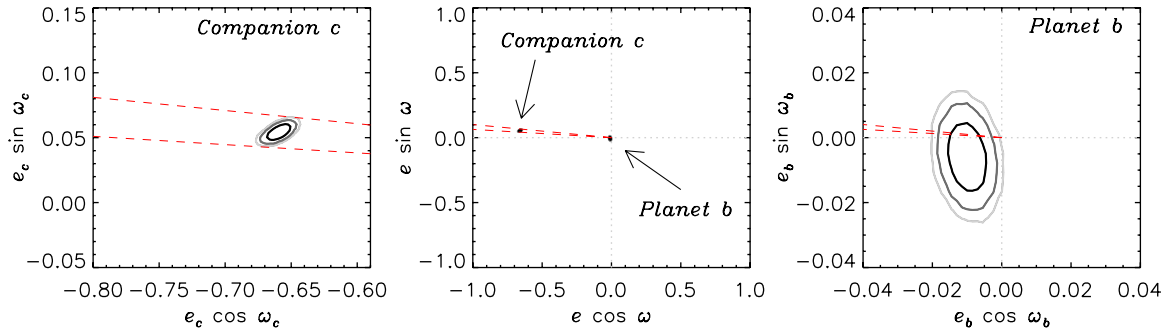

Figure 5. Results for the orbital eccentricities. The middle panel displays the results for b and c, while the left and right panels zoom in on the results of each object. The contours enclose 68%, 95%, and 99.73% of the MCMC samples. The dashed lines show the 99.73% confidence range for the apsidal orientation of c's orbit; they allow a visual assessment of the degree of apsidal alignment, and show that the limiting uncertainty in $\Delta\omega$ is the large uncertainty in $e_b \sin \omega_b$.

(A color version of this figure is available in the online journal.)

because they obey Gaussian distributions, while e obeys a Rayleigh distribution (see, e.g., Shen & Turner 2008). We found $e_b \cos \omega_b = -0.0099 \pm 0.0036$ (i.e., nonzero with 2.8σ significance) and $e_c \sin \omega_c = -0.0060 \pm 0.0069$. The eccentricity of b's orbit is right on the edge of detectability.[11]

Because of the low significance of this detection, it is impossible to draw a firm conclusion about whether its orbit is aligned with that of companion c. Our result is $\Delta\omega \equiv \omega_b - \omega_c = 36^{+27}_{-36}$ deg. The red dashed lines in Figure 5 show the 3σ allowed region for ω_c. The lines intersect the allowed region for planet b, as shown in the right panel. Most of the uncertainty in $\Delta\omega$ arises from the poorly determined orientation of b's orbit.[12]

The best way to check on the eccentricity of b's orbit would be to observe an occultation with the *Spitzer Space Telescope*. The timing of occultations would allow $e_b \cos \omega_b$ to be determined with an accuracy of about 0.001, several times better than the RV result. However, even after such an observation, considerable uncertainty would remain in $\Delta\omega$ because the accuracy in $e_b \sin \omega_b$ would not be much improved.

3.3. The Rossiter–McLaughlin Effect

The RV data obtained during transits exhibit a prograde RM effect: an anomalous redshift for the first half of the transit, followed by an anomalous blueshift for the second half. The fit to the data is shown in Figure 4, and the resulting constraints on λ and $v \sin i_\star$ are shown in Figure 6. The finding of $\lambda = 1.9 \pm 8.6$ deg implies a close alignment between the rotational angular momentum of the star, and the orbital angular momentum of the planet, at least as projected on the sky. Our result for the projected stellar rotation velocity, $v \sin i_\star = 1.66 \pm 0.37$ km s^{-1}, is about 1σ smaller than the result of 2.9 ± 1.0 km s^{-1} reported by Bakos et al. (2009).

3.4. Inferior Conjunction of Planet C

It is not yet known whether the inclination of c's orbit is close enough to 90° for transits to occur. Observations of transits would reveal the mass and radius of the companion, allow a more precise characterization of its orbit, and place constraints on the mutual inclination of orbits b and c.

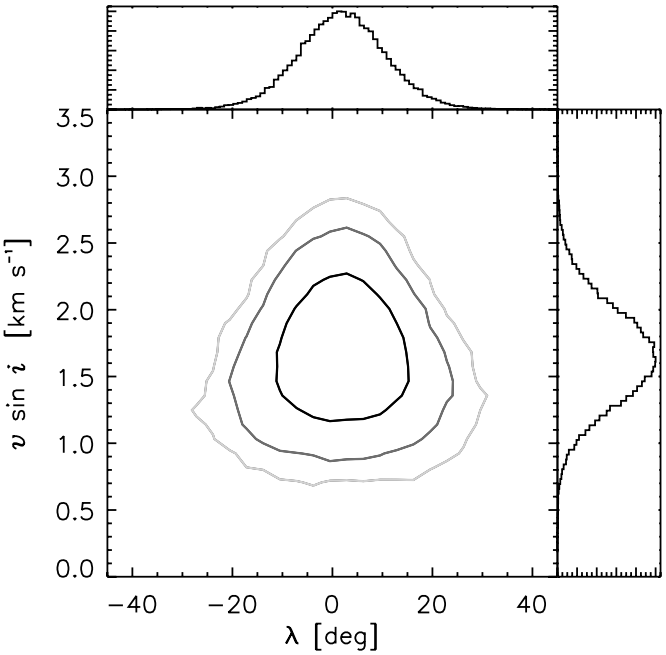

Figure 6. Results for the RM parameters, based on our MCMC analysis of the RV data. The contours represent 68%, 95%, and 99.73% confidence limits, and the one-dimensional (marginalized) posterior probability distributions are shown on the sides of the contour plot.

Using our results we predicted the times of inferior conjunctions of planet c, which is when transits would occur. The accuracy of the predicted time is limited by correlations with the uncertainties in c's velocity semiamplitude and eccentricity (see Figure 7). Table 3 gives the results. The quoted uncertainties represent 1σ (68.3%) confidence levels. It would be prudent to keep the star under continuous photometric surveillance for the entire 3σ time range, at least. The maximum transit duration is 14.9 hr.

4. DISCUSSION

HAT-P-13 was already a noteworthy system, as the first known case of a star with a transiting planet and a second close companion. We have presented evidence for a third companion in the form of a long-term radial acceleration of the star. The properties of the newly discovered long-period companion will remain poorly known until additional RV data are gathered over a significant fraction of its orbital period. Our analysis of the RM effect shows that planet b's orbital axis is aligned with the stellar

[11] For this reason, the results are also sensitive to the choice of priors for the fitting parameters. The results described in this section and given in Table 2 are based on uniform priors for $e_b \cos \omega_b$ and $e_b \sin \omega_b$. If instead uniform priors are adopted for e_b and ω_b, then we find $e_b = 0.0119 \pm 0.0040$.

[12] If we *assume* the orbits are apsidally locked, and repeat the fitting procedure with the requirement $\Delta\omega = 0$, we find $e_b = 0.0104 \pm 0.0032$.

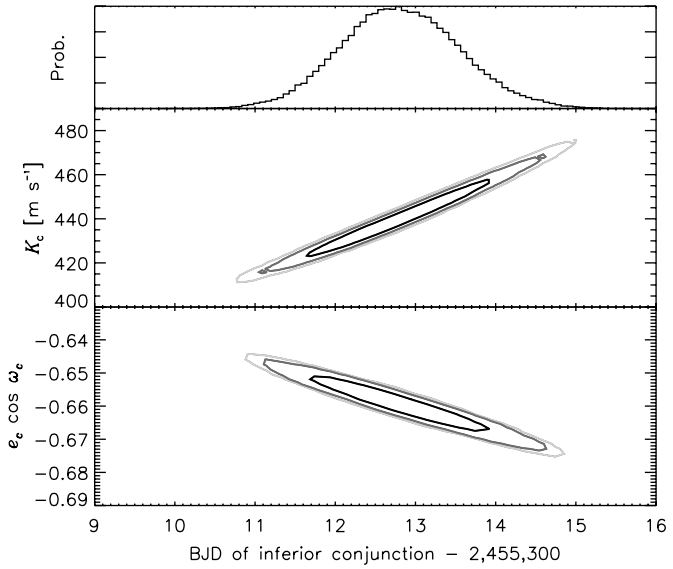

Figure 7. Results for the timing of the inferior conjunction of companion c, based on our MCMC analysis of the RV data. The top panel shows the one-dimensional (marginalized) posterior probability distribution. The lower two panels illustrate the correlation with the other poorly determined parameters of companion c. The contours represent 68%, 95%, and 99.73% confidence limits.

rotation axis, as projected on the sky. Our new data also agree with the previous finding that the orbit of planet b is slightly eccentric.

The latter two findings are relevant to the second reason why HAT-P-13 is noteworthy: its orbital configuration may represent an example of two-planet tidal evolution. In this scenario, first envisioned by Wu & Goldreich (2002) and investigated further by Mardling (2007), tidal circularization of the inner planet's orbit is delayed due to gravitational interactions with the outer planet. The interactions drive the system into a state of apsidal alignment, where it remains as both orbits are slowly circularized. As it turned out, the specific planetary system that inspired Wu & Goldreich (2002) was irrelevant to their theory, because the "outer planet" was found to be a spurious detection (Butler et al. 2002).

Batygin et al. (2009) welcomed HAT-P-13 as a genuine system that followed the path predicted by Wu & Goldreich (2002), and with the additional virtue that the inner planet is transiting. For this interpretation to be valid, the apsides of b and c must be aligned, whereas we have found the angle between the apsides to be 36^{+27}_{-36} deg, differing from zero by 1σ. We do not consider this result to be significant enough to draw a firm conclusion, especially in light of the uncertainties due to the ad hoc stellar jitter term and our simplified treatment of the influence of companion d. Further RV monitoring and observations of occultations are needed to make progress.

Batygin et al. (2009) also showed that the existence of transits would allow for an empirical estimate of the tidal Love number k_2 of planet b, as mentioned in Section 1. The requirement that the apsidal precession rates of b and c are equal leads to a condition on k_2, because b's precession rate is significantly affected by its tidal bulge. Subsequent work by Mardling (2010) showed that for a unique determination of k_2 it is necessary for the mutual inclination Δi between orbits b and c to be small. If instead the orbits are mutually inclined, then tidal evolution drives the system into a state in which e_b and Δi undergo oscillations: a cycle in parameter space, instead of a fixed point. Furthermore, Mardling (2010) argued that a large

Table 3
Predicted Times of Inferior Conjunction for HAT-P-13c

Year	Month	Date	Hour (UT)	Julian Date	Uncertainty (days)
2010	Apr	26	7.3	2,455,312.80	0.74
2011	Jul	16	13.9	2,455,759.08	0.85
2012	Oct	4	20.4	2,456,205.35	1.00
2013	Dec	25	3.0	2,456,651.62	1.17
2015	Mar	16	9.6	2,457,097.90	1.36

mutual inclination should be considered plausible, or even likely, given c's high eccentricity. She proposed that b and c began with nearly circular and coplanar orbits, but c's orbit was strongly perturbed by an interaction with a hypothetical outer planet. Those same perturbations would likely have tilted c's orbit.

The relation, if any, between the newly discovered HAT-P-13d and Mardling's hypothetical outer planet is unclear. In her scenario, the outer planet is ejected from the system. This seems important to the scenario, as otherwise d would continue interacting with c, and interfere with the tidal evolution of b and c. Thus, unless d's pericenter was somehow raised to avoid further encounters with c, it does not seem likely to have played the role envisioned by Mardling (2010). Of course the scenario could still be correct even if the third companion d was not the scattering agent; a fourth (ejected) companion may have been responsible.

Our study of the RM effect pertains to the angle $\psi_{\star,b}$ between planet b's orbit and the stellar equator, and has no *direct* bearing on the angle Δi between the orbital planes of b and c. However, there is an *indirect* connection, through the nodal precession that would be caused by mutually inclined orbits. As shown by Mardling (2010), planet b is far enough from the star that its orbital precession rate is likely to be dominated by the torque from c, rather than the quadrupole moment J_2 of the star. The critical orbital distance inside which the stellar torque is dominant is $\sim(2J_2a_c^2M_c/M_\star)^{0.2}$ (Burns 1986), which is 0.020 AU assuming $J_2 = 2 \times 10^{-7}$ as for the Sun. This is smaller than the actual orbital distance of 0.043 AU. Hence if Δi were large, then b's orbit would nodally precess around c's orbital axis, which would cause periodic variations in $\psi_{\star,b}$. Therefore, at any given moment in the system's history, we would be unlikely to observe a small value of $\psi_{\star,b}$ unless Δi were small. However, it is impossible to draw firm conclusions about Δi because of the dependence on initial conditions, the possible effects of companion d, and the fact that only the sky-projected angle λ is measured rather than the true obliquity $\psi_{\star,b}$.

It may be possible to estimate Δi based on transit-timing variations of planet b (Nesvorný & Beaugé 2010; Bakos et al. 2009). An even more direct estimate of Δi could be achieved if transits of c were detected. The existence of transits would show that i_c is nearly 90°, as is i_b. This would suggest Δi is small, although it would still be possible that the orbits are misaligned and their line of nodes happens to lie along the line of sight. The most definitive result would be obtained by observing the RM effect during transits of c, and comparing c's value of λ with that of planet b. In effect, the rotation axis of the star would be used as a reference line from which the orientation of each orbit is measured (Fabrycky 2009). This gives additional motivation to observe HAT-P-13 throughout the upcoming conjunctions of companion c.

We thank Dan Fabrycky for helpful conversations, especially about the dynamical implications of our results. We also

thank Debra Fischer and John Brewer for investigating the spectroscopic determination of the stellar rotation rate. We are grateful to Scott Gaudi and Greg Laughlin for comments on the manuscript.

J.N.W. gratefully acknowledges support from the NASA Origins program through award NNX09AD36G and the MIT Class of 1942. A.W.H. acknowledges a Townes Postdoctoral Fellowship from the Space Sciences Laboratory at UC Berkeley. G.A.B. was supported by NASA grant NNX08AF23G and an NSF Astronomy & Astrophysics Postdoctoral Fellowship (AST-0702843). G.T. acknowledges partial support from NASA grant NNX09AF59G. S.A. acknowledges the support of the Netherlands Organisation for Scientific Research (NWO). N.N. was supported by a Japan Society for Promotion of Science (JSPS) Fellowship for Research (PD: 20-8141). J.N.W. and N.N. were also supported in part by the National Science Foundation under Grant No. NSF PHY05-51164 (KITP program "The Theory and Observation of Exoplanets" at UCSB).

The data presented herein were obtained at the W. M. Keck Observatory, which is operated as a scientific partnership among the California Institute of Technology, the University of California, and the National Aeronautics and Space Administration, and was made possible by the generous financial support of the W. M. Keck Foundation. We extend special thanks to those of Hawaiian ancestry on whose sacred mountain of Mauna Kea we are privileged to be guests. Without their generous hospitality, the Keck observations presented herein would not have been possible.

Facilities: Keck:I (HIRES)

REFERENCES

Bakos, G. Á., et al. 2009, ApJ, 707, 446
Batygin, K., Bodenheimer, P., & Laughlin, G. 2009, ApJ, 704, L49
Burns, J. 1986, in Satellites, ed. J. Burns & M. Matthews (Tucson, AZ: Univ. Arizona Press), 117
Butler, R. P., Marcy, G. W., Williams, E., McCarthy, C., Dosanjh, P., & Vogt, S. S. 1996, PASP, 108, 500
Butler, R. P., et al. 2002, ApJ, 578, 565
Claret, A. 2004, A&A, 428, 1001
Correia, A. C. M., et al. 2010, A&A, 511, A21
Fabrycky, D. C. 2009, in IAU Symp. 253, Transiting Planets, ed. F. Pont, D. Sasselov, & M. Holman (Cambridge: Cambridge Univ. Press), 173
Gaudi, B. S., & Winn, J. N. 2007, ApJ, 655, 550
Howard, A. W., et al. 2009, ApJ, 696, 75
Léger, A., et al. 2009, A&A, 506, 287
Mandel, K., & Agol, E. 2002, ApJ, 580, L171
Mardling, R. A. 2007, MNRAS, 382, 1768
Mardling, R. A. 2010, MNRAS, in press (arXiv:1001.4079)
Narita, N., et al. 2010, PASJ, 62, 779
Nesvorný, D., & Beaugé, C. 2010, ApJ, 709, L44
Ohta, Y., Taruya, A., & Suto, Y. 2005, ApJ, 622, 1118
Pál, A. 2008, MNRAS, 390, 281
Pál, A., et al. 2008, ApJ, 680, 1450
Queloz, D., et al. 2009, A&A, 506, 303
Shen, Y., & Turner, E. L. 2008, ApJ, 685, 553
Vogt, S. S., et al. 1994, Proc. SPIE, 2198, 362
Winn, J. N., Holman, M. J., & Fuentes, C. I. 2007, AJ, 133, 11
Winn, J. N., Johnson, J. A., Albrecht, S., Howard, A. W., Marcy, G. W., Crossfield, I. J., & Holman, M. J. 2009, ApJ, 703, L99
Winn, J. N., et al. 2005, ApJ, 631, 1215
Wright, J. T. 2005, PASP, 117, 657
Wright, J. T. 2010, EAS Publ. Ser., 42, 3
Wu, Y., & Goldreich, P. 2002, ApJ, 564, 1024